PHYSICAL REVIEW C **88**, 041001(R) (2013)

Search for evidence of ${}^{3}_{\Lambda}n$ by observing $d + \pi^-$ and $t + \pi^-$ final states in the reaction of ^{6}Li + ^{12}C at 2A GeV

C. Rappold,[1,2,*] E. Kim,[1,3] T. R. Saito,[1,4,5,†] O. Bertini,[1,4] S. Bianchin,[1] V. Bozkurt,[1,6] M. Kavatsyuk,[7] Y. Ma,[1,4] F. Maas,[1,4,5] S. Minami,[1] D. Nakajima,[1,8] B. Özel-Tashenov,[1] K. Yoshida,[1,5,9] P. Achenbach,[4] S. Ajimura,[10] T. Aumann,[1,11] C. Ayerbe Gayoso,[4] H. C. Bhang,[3] C. Caesar,[1,11] S. Erturk,[6] T. Fukuda,[12] B. Göküzüm,[1,6] E. Guliev,[7] J. Hoffmann,[1] G. Ickert,[1] Z. S. Ketenci,[6] D. Khaneft,[1,4] M. Kim,[3] S. Kim,[3] K. Koch,[1] N. Kurz,[1] A. Le Fèvre,[1,13] Y. Mizoi,[12] L. Nungesser,[4] W. Ott,[1] J. Pochodzalla,[4] A. Sakaguchi,[9] C. J. Schmidt,[1] M. Sekimoto,[14] H. Simon,[1] T. Takahashi,[14] G. J. Tambave,[7] H. Tamura,[15] W. Trautmann,[1] S. Voltz,[1] and C. J. Yoon[3]

(HypHI Collaboration)

[1]*GSI Helmholtz Centre for Heavy Ion Research, Planckstrasse 1, 64291 Darmstadt, Germany*
[2]*Justus-Liebig-Universität Giessen, Heinrich-Buff-Ring 16, 35392 Giessen, Germany*
[3]*Seoul National University, Gwanakro Sillim-dong, Gwanak-gu, Seoul 151-747, Republic of Korea*
[4]*Johannes Gutenberg-Universität Mainz, J. J. Becherweg 40, 55099 Mainz, Germany*
[5]*Helmholtz Institute Mainz (HIM), J. J. Becherweg 40, 55099 Mainz, Germany*
[6]*Nigde University, 51100 Nigde, Turkey*
[7]*KVI, University of Groningen, Zernikelaan 25, NL-9747 AA Groningen, The Netherlands*
[8]*University of Tokyo, 7-3-1 Hongo, Bunkyo-ku, Tokyo 113-0033, Japan*
[9]*Osaka University, 1-1 Machikaneyama, Toyonaka, Osaka 560-0043, Japan*
[10]*Research Centre for Nuclear Physics (RCNP), 10-1 Mihogaoka, Ibaraki, Osaka 567-0047, Japan*
[11]*Technische Universität Darmstadt, 64289 Darmstadt, Germany*
[12]*Osaka Electro-communication University, Hatsu-cho 18-8, Neyagawa, Osaka 572-8530, Japan*
[13]*SUBATECH, La Chantrerie, 4 rue Alfred Kastler, BP 20722, 44307 Nantes cedex 3, France*
[14]*KEK, 1-1 Oho, Tsukuba, Ibaraki 305-0801, Japan*
[15]*Tohoku University, 6-3 Aoba Aramaki Aoba Sendai, Miyagi 980-7875, Japan*

(Received 23 June 2013; published 10 October 2013)

The experimental data obtained from the reaction of ^{6}Li projectiles at 2A GeV on a fixed graphite target were analyzed to study the invariant mass distributions of $d + \pi^-$ and $t + \pi^-$. Indications of a signal in the $d + \pi^-$ and $t + \pi^-$ invariant mass distributions were observed with significances of 5.3 σ and 5.0 σ, respectively, when including the production target, and 3.7 σ and 5.2 σ, respectively, when excluding the target. The estimated mean values of the invariant mass for $d + \pi^-$ and $t + \pi^-$ signal were 2059.3 $\pm$ 1.3 $\pm$ 1.7 MeV/c^2 and 2993.7 $\pm$ 1.3 $\pm$ 0.6 MeV/c^2 respectively. The lifetime estimation of the possible bound states yielding to $d + \pi^-$ and $t + \pi^-$ final states were deduced to be as $181^{+30}_{-24} \pm 25$ ps and $190^{+47}_{-35} \pm 36$ ps, respectively. Those final states may be interpreted as the two-body and three-body decay modes of a neutral bound state of two neutrons and a Λ hyperon, ${}^{3}_{\Lambda}n$.

DOI: 10.1103/PhysRevC.88.041001 PACS number(s): 21.80.+a, 25.70.Mn

A hypernucleus, a subatomic system with at least one bound hyperon, is studied in order to deduce the information about fundamental hyperon (Y)–nucleon (N) and Y-Y interactions. Hypernuclei have been mainly studied by means of the missing-mass experiments with secondary-meson and primary-electron beams [1] and earlier with emulsion techniques and bubble chambers [2]. In these experiments, a variety of hypernuclei with the lightest hyperon, the Λ hyperon, were produced and identified. However, the isospin of the produced Λ hypernuclei is similar to that of the target nucleus in these experiments, since they are produced by the elementary process of converting one nucleon in the target nucleus into a Λ hyperon.

Information on the Λ-N interaction was already inferred from the hypernuclei in the vicinity of the β stability line [3–6]. The nature of the Λ-N interaction for neutron-rich hypernuclei, in which the ΛN-ΣN coupling three-body force may play a role as described theoretically in Refs. [7–11], has not yet been studied in detail since only a few cases were observed, ${}^{10}_{\Lambda}$Li [12], ${}^{7}_{\Lambda}$He [13], and ${}^{6}_{\Lambda}$H [14]. We thus search for other neutron-rich hypernuclei by means of induced reactions of heavy-ion beams.

Neutron- and proton-rich hypernuclei can be indeed studied by using projectile fragmentation reactions of heavy-ion beams. In such reactions, a projectile fragment can capture a hyperon produced in the hot participant region to produce a hypernucleus [15–19]. They might also be produced in a multistage process, such as through a Fermi breakup decay of excited heavier hypernuclear spectators, possibly formed in peripheral collisions [19–21].

We, the HypHI Collaboration, have proposed a series of experiments at the GSI Helmholtz Centre for Heavy Ion Research that would use induced reactions of stable heavy-ion beams and rare-isotope beams to produce

*c.rappold@gsi.de
†t.saito@gsi.de

and identify hypernuclei by means of the invariant mass method [22].

We performed an experiment with ^{6}Li projectiles at 2A GeV with an intensity of 3×10^{6} ion per second bombarding on a carbon (^{12}C) graphite target with a thickness of 8.84 g/cm^{2}. The data collection occurred during a period of 3.5 days with an integrated luminosity of 0.066 pb^{-1}. The main goal of the experiment was to identify and study the production and the decay of light hypernuclei, $^{3}_{\Lambda}$H and $^{4}_{\Lambda}$H, as well as Λ hyperons in order to demonstrate the feasibility of such hypernuclear spectroscopy. Within the same data set other possible final states can be studied to search for extremely neutron-rich and neutral hypernuclei such as a bound state of two neutrons with a Λ hyperon, $^{3}_{\Lambda}n$. The observation of a $^{3}_{\Lambda}n$ state was not feasible in the previous emulsion technique and bubble chamber experiments since this bound state has no charge and could not be distinguished from the background induced by the Λ hyperon. Garcilazo *et al.* studied theoretically the $nn\Lambda$ state and revealed that it should be unbound [23]; however, recent lattice QCD calculations for three-body states [24] indicate that $^{3}_{\Lambda}n$ might be bound. Additional considerations from Dalitz and Downs [25] show possible decay channels of such a state, $^{3}_{\Lambda}n \rightarrow p + n + n + \pi^{-}$ and $^{3}_{\Lambda}n \rightarrow t + \pi^{-}$ and the first calculation on its binding energy. In a revised calculation presented in Ref. [26], they concluded again that the existence of $^{3}_{\Lambda}n$ was improbable. In the later publication by Dalitz and Levi Setti on the possible unusual light hypernuclei [27], the possibility of $^{3}_{\Lambda}n$ existence was still discarded; however, experimental evidences were welcome, and they discussed the possibilities of $^{5}_{\Lambda}n$ and $^{4}_{\Lambda}n$ as well.

The experiment involved tracking systems of scintillating fiber detector arrays and two drift chambers for the secondary vertex determination. Four scintillating hodoscope walls were adjoined to the tracking systems for tracking and time-of-flight measurements of charged particles across a large acceptance dipole magnet. The tracking system for vertexing was placed in front of the dipole magnet around the expected decay volume of hypernuclei. Behind the magnet, two separated arms of the detection apparatus were situated in such a way to measure disjointedly positively and negatively charged particles.

The four-vectors of the detected particles and fragments were determined after the particle identification based on tracking across the magnet as well as measurements of the time-of-flight and the energy deposit with the hodoscope walls. After the decay vertex finding, the invariant mass of final states of interest was calculated, and a lifetime estimation was inferred based on the observed decay vertex position. The feasibility of the experimental method was already demonstrated by observing Λ, $^{3}_{\Lambda}$H, and $^{4}_{\Lambda}$H, whose physics results are discussed in Ref. [28]. In this Rapid Communication, we report on the analyses and discussions of the observed final states of $d + \pi^{-}$ and $t + \pi^{-}$ that might be associated with $^{3}_{\Lambda}n$.

Using the track and event reconstruction procedures, the particle identification for positively charged fragments was first determined by the correlation between the measured energy deposit and the deduced momentum from the track fitting. The performance for the helium isotope separation was reasonable, and the ^{3}He contamination in the ^{4}He identification was estimated to be 1.7%, while the contamination of ^{4}He into the identification of ^{3}He was 1.8% [28]. Additionally, for the hydrogen isotopes and π^{-} mesons the correlation between the estimated momentum and the velocity β calculated from the time-of-flight measurement was employed, as detailed in Ref. [28]. The selection cuts used for the deuteron and triton determination required their respective momenta to fall in the ranges 4.3 $\sim$ 6.5 and 6.5 $\sim$ 10.0 GeV/c and their respective masses to be within $0.935 < m_{d} < 2.785$ and $1.455 < m_{t} < 4.105$ GeV/c^{2}. A fair separation between the hydrogen isotopes was achieved. The contamination of protons and tritons in the deuteron selection is 0.75% and 2.7%, respectively. For the triton selection the proton contamination was negligible, while the deuteron contamination amounted to 1.9%. Cut conditions for triton and deuteron species were wide enough so that there is no narrowing of the projectile rapidity region, cross-checked with the rapidity regions of detected helium and lithium isotopes.

After the identification of the particles and fragments of interest, the invariant mass distributions of $d + \pi^{-}$ and $t + \pi^{-}$ were studied with the identical rules for the secondary vertex selections applied in the case of Λ, $^{3}_{\Lambda}$H, and $^{4}_{\Lambda}$H [28]. Figure 1 shows the resultant invariant mass distributions of $d + \pi^{-}$ in panels (a1) and (a2) and $t + \pi^{-}$ in panels (b1) and (b2). The longitudinal decay vertex position (Z) was requested to be set

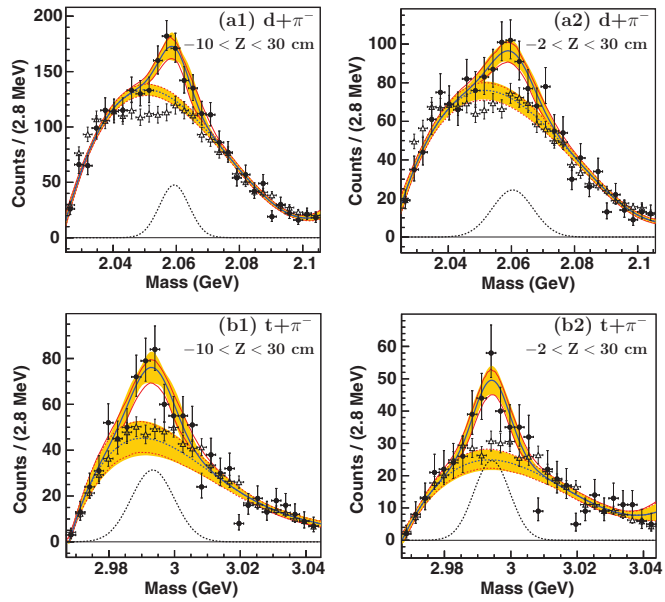

FIG. 1. (Color online) Invariant mass distributions of $d + \pi^{-}$ final-state candidate in panels (a1) and (a2) and of $t + \pi^{-}$ in panels (b1) and (b2). Panels (a1) and (b1) are for -10 cm $< Z <$ 30 cm, and panels (a2) and (b2) are for -2 cm $< Z <$ 30 cm. Observed distributions are represented by the filled-in circles. The hashed orange (gray) region represents one standard deviation of the fitted model centered at the solid blue (gray) line of the total best fit. The black and colored dotted lines respectively show the separate contributions of the signal and the background. The open triangle represents the data corresponding to invariant mass distribution of the mixed event analysis.

TABLE I. Summary of the estimation of the model parameters of the invariant mass distribution fit with the cut condition of -10 cm $< Z <$ 30 cm. The parameter $N_{\rm sig}$ represents the integral of the signal contribution without efficiency and acceptance corrections, while N_{bg} represents that of the background contributions. The mean value, $\bar{m}$, and the standard deviation, σ_m, of the Gaussian model of the signal are also summarized. For $\bar{m}$, the first error value is statistical, and the second one is deduced by the propagation of the uncertainty in the mass calibration.

Fitted values	$d+\pi^-$	$t+\pi^-$
$N_{\rm sig}$	202 ± 67	181 ± 92
$\bar{m}$ (MeV/c^2)	2059.3 ± 1.3 ± 2.6	2993.7 ± 1.3 ± 2.3
σ_m (MeV/c^2)	4.7 ± 1.7	6.5 ± 2.4
N_{bg}	2298 ± 81	748 ± 92

between -10 cm $< Z <$ 30 cm in Figs. 1(a1) and 1(b1) and between -2 cm $< Z <$ 30 cm in Figs. 1(a2) and 1(b2). The production target was placed between -6 and -2 cm, thus the cut condition of -10 cm $< Z <$ 30 cm includes vertices from the production target while the other condition excludes the target region. The deduced invariant mass distributions are represented by the filled-in circles. The mass values were calibrated by using the data for the reconstructed invariant mass peak positions of Λ, ${}^{3}_{\Lambda}$H, and ${}^{4}_{\Lambda}$H.

The procedures for fitting and hypothesis testing were based on the ROOFIT and ROOSTATS frameworks [29,30], which have been already applied for the analysis on Λ, ${}^{3}_{\Lambda}$H, and ${}^{4}_{\Lambda}$H [28]. A binned maximum likelihood fit was performed to the $d+\pi^-$ and $t+\pi^-$ invariant mass spectra. The fitting model was a combination of a Gaussian probability density function and a Chebychev polynomial probability density function of the first kind, for signal and background contributions respectively. No parameters of the full model were constrained for the extended binned maximum likelihood fit. The degree of Chebychev polynomial function for the background contribution was selected by F tests over the different resultant fitted models in order to judge whether an additional parameter to the model would overfit the data. The selected fitted model constrained more robustly the background contribution in such a way that a more conservative model for the fit would not overestimate the significance of the signal contribution. The hashed orange (gray) region represents one standard deviation of the fitted model centered at the solid blue (gray) line of the total best fit. The fitted results, omitting the parameters for the Chebychev polynomial function, are listed in Tables I and II for both cut conditions on the decay vertex position. In addition, the estimation of the background using the event mixing method is shown by the open triangles in Fig. 1. By hypothesis testing via profiled likelihood ratio tests, the significance values of observed peaks of $d+\pi^-$ for -10 cm $< Z <$ 30 cm and -2 cm $< Z <$ 30 cm were determined to be respectively 5.3 and 3.7 σ, and for $t+\pi^-$ they are 5.0 and 5.2 σ, respectively.

TABLE II. Summary of the results obtained by the model fitting for the invariant mass distributions with the cut condition of -2 cm $< Z <$ 30 cm. Conventions are same as in Table I.

Fitted values	$d+\pi^-$	$t+\pi^-$
$N_{\rm sig}$	143 ± 64	118 ± 41
$\bar{m}$ (MeV/c^2)	2060.4 ± 1.7 ± 2.7	2994.3 ± 1.1 ± 2.2
σ_m (MeV/c^2)	6.5 ± 2.3	5.4 ± 1.4
N_{bg}	1429 ± 74	431 ± 41

The invariant mass value was calibrated as explained above from the measured mass of the Λ, ${}^{3}_{\Lambda}$H, and ${}^{4}_{\Lambda}$H. A multisim approach was employed for simulating the simultaneous effects of parameter uncertainties of the calibration function [31,32], in order to estimate the systematic uncertainty induced by the uncertainty of their peak positions [28]. An ensemble of Monte Carlo samples was created in which all calibration parameters were chosen randomly in respect to their covariance matrix and applied to the data set. The total effect of the system was then extracted from the distribution of the obtained mean value, $\bar{m}$, after the maximum likelihood fit procedure. The systematic uncertainty on the mean value $\bar{m}$ of the model is reported as the second error quoted in Tables I and II.

The lifetime values of the final states of $d+\pi^-$ and $t+\pi^-$ were estimated via an unbinned maximum likelihood fitting method in which the signal-plus-background region and the background-only sidebands were used to determine the contribution of the signal and background to the proper decay time distribution. The method was already examined

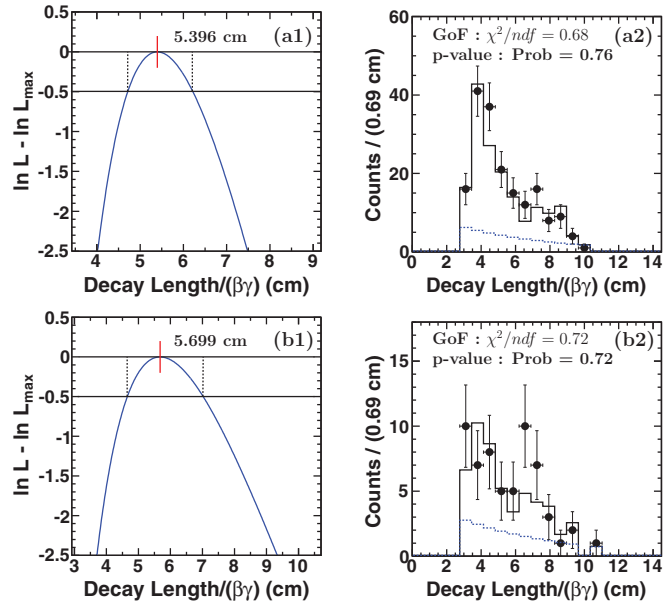

FIG. 2. (Color online) Profiled likelihood ratio for interval estimation of the lifetime of $d+\pi^-$ (a1) and $t+\pi^-$ (b1) final states. Interval estimation for one standard deviation is shown on each profiled likelihood ratio. *Binned* decay length distributions of the signal region of $d+\pi^-$ (a2) and $t+\pi^-$ (b2) are shown with the fitted model. The model includes the exponential function that resulted from the *unbinned* maximum likelihood fit and the background contribution estimated by the sidebands. The fitted model is represented by the black line, while the contribution of the exponential function is represented by the dotted blue (gray) line.

TABLE III. Contributions to the systematic uncertainties of the lifetime estimation. The contribution from the different boundary ranges of the longitudinal vertex position cut is denoted as "vertex Z pos". The contribution from the uncertainty of the primary vertex position shown as the "primary vertex". The contribution from the effect of the scaling factor between the background contribution from the sidebands and the signal region is represented by "scaling". The contribution from the different sideband regions for the background contribution is denoted as "sideband". The last row indicates the share of the total systematic error.

Contribution to the systematic	$d+\pi^-$	$t+\pi^-$
Vertex Z pos (%)	12	17
Primary vertex (%)	4	4
Scaling (%)	7	6
Sideband (%)	2	2
Total (%)	14	19

by deducing our measured lifetime of Λ hyperon [28] being consistent with the known value of 263.2 ± 2.0 ps [33]. The lifetime values of ${}^{3}_{\Lambda}$H and ${}^{4}_{\Lambda}$H were also extracted by the same procedure, and they were in good agreement with previous measurements [28].

For $d+\pi^-$ and $t+\pi^-$ final states, the profiled likelihood ratios for estimating the one-standard-deviation interval (68.3% CL) are shown respectively in Figs. 2(a1) and 2(b1). Resultant lifetime values with the $d+\pi^-$ and $t+\pi^-$ final states are respectively 181^{+30}_{-24} ps and 190^{+47}_{-35} ps. To represent the fitted values, the *binned* data of proper decay length in the signal region are displayed with the fitted model. The model includes the binned contribution of the exponential probability density function added to the *binned* data of the sideband regions [28]. These distributions are shown in Fig. 2, in panel (a2) for $d+\pi^-$ and in panel (b2) for $t+\pi^-$. The goodness of fit is tested by calculating the reduced χ^2 of the model decay length function over the *binned* data, as shown in these panels. The values of reduced χ^2 are 0.68 for $d+\pi^-$ and 0.72 for $t+\pi^-$.

The systematic uncertainties in deducing the lifetime values were also investigated as in Ref. [28], and they are summarized in Table III. First, the boundary range of the longitudinal vertex position selection cut had influence on the data sample's size and on the fitting procedure. Therefore, its contribution to the systematic uncertainty was estimated and listed in the second row of Table III (vertex Z pos). Variations on the primary vertex can be studied to determine possible systematic influence to lifetime uncertainty, as listed in the third row of Table III (primary vertex). The systematic effect of the scaling factor between the sidebands and the signal region was as well examined and listed in the fourth row (scaling). The position of the sideband regions for the estimation of the background estimation also yielded to another few percentage points of systematic uncertainty, as listed in the fifth row (sideband). The total systematic errors are respectively 14% and 19% for $d+\pi^-$ and $t+\pi^-$ final states.

Two points have to be investigated in order to interpret the obtained signals. First, one has to demonstrate that the analysis method does not create signals by itself. Second, one has to check whether multibody decays of other hypernuclei can induce such signals.

For the first point, by using an event generator based on the UrQMD calculations [34], an identical analysis was performed on the data produced by full GEANT4 Monte Carlo simulations in order to check whether the cut conditions in the analysis might induce a peak signal in the invariant mass distributions. In each generated event, mesons, baryons, and fragments that can be produced in the reaction ${}^{6}\mathrm{Li}+{}^{12}\mathrm{C}$ at $2A$ GeV were present, which eventually include π^-, Λ, deuterons, and tritons. Hypernuclei were as well generated in such a way that the kimenatics was conserved. The ${}^{3}_{\Lambda}$H, ${}^{4}_{\Lambda}$H, ${}^{4}_{\Lambda}$He, and ${}^{5}_{\Lambda}$He hypernuclei were also present in the generated events. No bound state finalizing $d+\pi^-$ and $t+\pi^-$ is present, thus no signal should be observed. The output of the UrQMD calculations were then considered as the primary vertex source of the ${}^{6}\mathrm{Li}+{}^{12}\mathrm{C}$ reaction in the GEANT4 simulations. The weak decay of hyperons and hypernuclei and the strong decay of resonances were handled by the GEANT4 framework. In those conditions, several possible sources for deuteron, triton, and π^- were used for the invariant mass reconstruction of $d+\pi^-$ and $t+\pi^-$ final states. The GEANT4 simulations provided the digitizations of the different detector information close to the real detector resolutions. The data structures out of the detector digitizers were written in a way similar to the structure of experimental data. The generated data were then fed to the track and event reconstruction analysis code without any modification. The investigated sources of $d+\pi^-$ and $t+\pi^-$ were deuteron and triton from the primary vertex of the ${}^{6}\mathrm{Li}+{}^{12}\mathrm{C}$ reaction. The investigated sources of π^- were from the primary vertex and from the weak decay of hyperons and hypernuclei of interest. The black dots in Fig. 3 show the invariant mass distributions with the simulated data for $d+\pi^-$ (a) and $t+\pi^-$ (b). The results of the mixed event analysis that was also performed on the simulated data are displayed as crossed red (gray) points. No peak structure raised by the cut conditions can be observed, as shown in the bottom panel of Fig. 3 by the plot of the ratio between the invariant mass distribution obtained from the Monte Carlo event data set and its associated event mixing analysis.

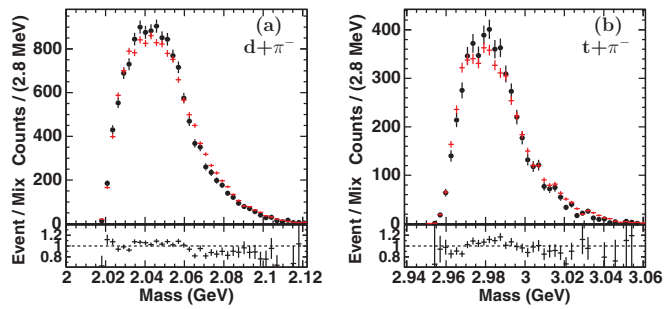

FIG. 3. (Color online) Invariant mass distribution for (a) $d+\pi^-$ and (b) $t+\pi^-$ from the GEANT4 Monte Carlo simulation data set, with the events produced by UrQMD represented by black symbols. Red (gray) crosses represent distributions with the mixed event analysis. The ratios between the both two distributions are shown in the bottom panel.

The second point was also investigated, i.e., whether the observed $d+\pi^-$ and $t+\pi^-$ signals can be originated from the three-body and four-body decays of ${}^{3}_{\Lambda}$H, ${}^{4}_{\Lambda}$H, ${}^{4}_{\Lambda}$He, ${}^{5}_{\Lambda}$He, and ${}^{6}_{\Lambda}$He, that are likely to be produced in the reaction. A mis-reconstruction of these decay modes may occur by observing only two among of the three or four daughter particles. For instance, in the three-body decay of ${}^{3}_{\Lambda}\mathrm{H}\rightarrow p+d+\pi^-$, the proton and deuteron could be produced via a two-body decay mode of ${}^{3}\mathrm{He}^*+\pi^-$ where ${}^{3}\mathrm{He}^*$ (the asterisk means an unbound state) is dissociated into $p+d$ with a small relative momentum. Theoretical study of this experimental phenomenon was performed and described in Ref. [35], and a similar experimental behavior in the three-body decay of ${}^{5}_{\Lambda}$He was also studied theoretically [36,37]. Peaks of $d+\pi^-$ or $t+\pi^-$ might be produced even though one daughter particle is omitted in the reconstruction. Those scenarios were tested by Monte Carlo simulations based on the phase space decay (code for the CERNLIB [38] inside of ROOT framework). It was shown that in the case of a chain of a two consecutive two-body decay ($a\rightarrow b+c$ then $b\rightarrow d+e$) in which the second two-body decay has a small relative momentum transfer, i.e., small Q value, the invariant mass of two out of three particles ($c+d$ or $c+e$) does produce a peak signal in the observable spectrum. Because of the small Q value in the second decay, the daughter particles or fragments (d and e) have very similar momentum directions as their mother (b) in the laboratory frame after the Lorentz boost of the center-of-mass frame of the mother (b).

The possible contributions to the $d+\pi^-$ and $t+\pi^-$ signals from the mis-reconstruction of these decay channels shown in Table IV can be estimated from the experimental data. The calculation is based on the peak integral of observed hypernuclear two-body decay in the same data set, on the trigger and detector efficiencies, and on the known branching ratios of the decay channels of Table IV. In the case of ${}^{3}_{\Lambda}$H and ${}^{4}_{\Lambda}$H the possible contributions in the observed $d+\pi^-$ and $t+\pi^-$ signals were calculated by using the observed peak integral of the two-body decay of ${}^{3}_{\Lambda}\mathrm{H}\rightarrow{}^{3}\mathrm{He}+\pi^-$ and ${}^{4}_{\Lambda}\mathrm{H}\rightarrow{}^{4}\mathrm{He}+\pi^-$ [28]. In the case of ${}^{6}_{\Lambda}\mathrm{He}\rightarrow{}^{6}\mathrm{Li}^*+\pi^-\rightarrow{}^{4}\mathrm{He}+d+\pi^-$, the observed upper limit in the ${}^{6}\mathrm{Li}+\pi^-$ invariant mass distribution and a branching ratio of three-body to two-body decays were used to estimate its possible contribution to the $d+\pi^-$ signal. ${}^{4}_{\Lambda}$He and ${}^{5}_{\Lambda}$He were not observed in the analysis since they do not have two-body decay channels and the efficiency for the three-body decay reconstruction is an order of magnitude lower than that for the two-body decay. Therefore, we calculated the contribution of ${}^{4}_{\Lambda}$He and ${}^{5}_{\Lambda}$He by estimating the upper limit of their production cross sections from the experimental data. Then we assessed an order of magnitude higher to their production cross sections to estimate the worst-case scenario. One can remark that the estimated contributions from all of those three- and four-body decay channels shown in Table IV are far smaller than the observed $d+\pi^-$ and $t+\pi^-$ signal counts in Table I.

TABLE IV. Possible contributions to $d+\pi^-$ and $t+\pi^-$ signals from the hypernuclear mesonic weak decay channels.

Decay channel	Branching ratios	Counts
${}^{3}_{\Lambda}\mathrm{H}\rightarrow p+d+\pi^-$	[35]	8 to $d+\pi^-$
${}^{4}_{\Lambda}\mathrm{H}\rightarrow d+d+\pi^-$	[39,40]	1 to $d+\pi^-$
${}^{4}_{\Lambda}\mathrm{H}\rightarrow t+p+\pi^-$	[39,40]	6 to $t+\pi^-$
${}^{6}_{\Lambda}\mathrm{He}\rightarrow{}^{4}\mathrm{He}+d+\pi^-$	[41]	3 to $d+\pi^-$
${}^{4}_{\Lambda}\mathrm{He}\rightarrow p+p+d+\pi^-$	[40,42]	8 to $d+\pi^-$
${}^{5}_{\Lambda}\mathrm{He}\rightarrow d+{}^{3}\mathrm{He}+\pi^-$	[40,43,44]	1 to $d+\pi^-$

In conclusion, a signal in the invariant mass distributions of $d+\pi^-$ and $t+\pi^-$ final states was observed. In addition, the decay into $d+\pi^-$ and $t+\pi^-$ can be attributed to strangeness-changing weak interaction since the extracted lifetimes, $181^{+30}_{-24}\pm 25$ ps and $190^{+47}_{-35}\pm 36$ ps, respectively, are similar to a typical weak decay process involving strangeness (an order of hundreds of ps). The HIRES Collaboration reported in Refs. [45,46] that no $S=-1$ dibaryon resonance (Λp) was encountered in the analysis of their missing-mass experiment in the reaction $p+p\rightarrow\mathrm{K}^+ + (\Lambda p)$. Furthermore the recent review from Gal [47] gives possible structures of a $S=-1$ dibaryon, excluding (Λp) possibility. In the review from Dalitz and Downs [25], a Λ-nucleon bound state is discarded. Those considerations may exclude the hypothesis that the $d+\pi^-$ final state originates from a $n\Lambda$ bound state.

A possible interpretation for the observed $t+\pi^-$ and $d+\pi^-$ final states might be the two- and three-body decays of an unknown bound state of two neutrons associated with Λ, ${}^{3}_{\Lambda}n$, via ${}^{3}_{\Lambda}n\rightarrow t+\pi^-$ and ${}^{3}_{\Lambda}n\rightarrow t^*+\pi^-\rightarrow d+n+\pi^-$, respectively. With this interpretation, the production mechanism of ${}^{3}_{\Lambda}n$ might be the Fermi breakup of excited heavier hyperfragments, and ${}^{3}_{\Lambda}n$ might not likely be produced by direct coalescence of a Λ hyperon and a dineuteron state in the projectile rapidity region since the dineutron state is known to be unbound. The existence of such a bound state is to be studied further experimentally and theoretically.

The authors thank the GSI Departments of Accelerator, Experimental Electronics, the Detector Laboratory, and the Target Laboratory and the Electronics Department of the Institute for Nuclear Physics of Mainz University for supporting the project. The HypHI project is funded by the Helmholtz Association as Helmholtz-University Young Investigators Group VH-NG-239 at GSI and the German Research Foundation (DFG) under Contract No. SA 1696/1-1. The authors acknowledge the financial support provided by the Ministry of Education, Science, and Culture of Japan, Grant-in-Aid for Scientific Research on Priority Areas 449, and Grant-in-Aid for promotion of Cooperative Research in Osaka Electro-communication University (2004–2006). This work is also supported by the Ministry of Education, Science, and Culture of Japan, Grants-in-Aid for Scientific Research 18042008 and EU FP7 Hadron-Physics-2 SPHERE. A part of this work was carried out on the HIMSTER high-performance computing infrastructure provided by the Helmholtz-Institute Mainz. We also thank A. Botavina, A. Gal, K. D. Gross, N. Hermann, E. Hiyama, R. Klanner, K. Langanke, I. Mishustin, H. Nemura, J. Schaffner-Bielich, C. Scheidenberger, H. Stöcker, and J. Stroth for the involved discussions.

[1] O. Hashimoto and H. Tamura, Prog. Part. Nucl. Phys. **57**, 564 (2006).
[2] D. Davis, Nucl. Phys. A **754**, 3 (2005).
[3] H. Tamura *et al.*, Phys. Rev. Lett. **84**, 5963 (2000).
[4] K. Tanida *et al.*, Phys. Rev. Lett. **86**, 1982 (2001).
[5] M. Ukai *et al.*, Phys. Rev. Lett. **93**, 232501 (2004).
[6] M. Ukai *et al.*, Phys. Rev. C **77**, 054315 (2008).
[7] K. Miyagawa *et al.*, Few-Body Syst., Suppl. **12**, 324 (2000).
[8] Y. Akaishi, T. Harada, S. Shinmura, and K. S. Myint, Phys. Rev. Lett. **84**, 3539 (2000).
[9] E. Hiyama, M. Kamimura, T. Motoba, T. Yamada, and Y. Yamamoto, Phys. Rev. C **65**, 011301 (2001).
[10] H. Nemura, Y. Akaishi, and Y. Suzuki, Phys. Rev. Lett. **89**, 142504 (2002).
[11] A. Nogga, H. Kamada, and W. Glockle, Phys. Rev. Lett. **88**, 172501 (2002).
[12] P. Saha *et al.*, Phys. Rev. Lett. **94**, 052502 (2005).
[13] S. Nakamura *et al.*, Phys. Rev. Lett. **110**, 012502 (2013).
[14] M. Agnello *et al.*, Phys. Rev. Lett. **108**, 042501 (2012).
[15] A. K. Kerman and M. S. Weiss, Phys. Rev. C **8**, 408 (1973).
[16] F. Asai, H. Bando, and M. Sano, Phys. Lett. B **145**, 19 (1984).
[17] H. Bando, M. Sano, J. Zofka, and M. Wakai, Nucl. Phys. A **501**, 900 (1989).
[18] T. Gaitanos, H. Lenske, and U. Mosel, Phys. Lett. B **675**, 297 (2009).
[19] A. Botvina, K. Gudima, J. Steinheimer, I. Mishustin, J. Pochodzalla, A. S. Lorente, M. Bleicher, and H. Stoecker, Nucl. Phys. A **881**, 228 (2012).
[20] A. Sanchez Lorente *et al.*, Phys. Lett. B **697**, 222 (2011).
[21] A. S. Botvina, I. N. Mishustin, and J. Pochodzalla, Phys. Rev. C **86**, 011601 (2012).
[22] T. Saito *et al.*, www.gsi-schwerionenforschung.org/documents/DOC-2005-Feb-432-1.ps.
[23] H. Garcilazo, A. Valcarce, and T. Fernandez-Carames, Phys. Rev. C **76**, 034001 (2007).
[24] S. Beane, E. Chang, S. Cohen, W. Detmold, H. Lin *et al.*, Phys. Rev. D **87**, 034506 (2013).
[25] R. H. Dalitz and B. W. Downs, Phys. Rev. **110**, 958 (1958).
[26] B. W. Downs and R. H. Dalitz, Phys. Rev. **114**, 593 (1959).
[27] R. Dalitz and R. Levi Setti, Nuovo Cimento **30**, 489 (1963).
[28] C. Rappold *et al.*, Nucl. Phys. A **913**, 170 (2013).
[29] W. Verkerke and D. Kirkby, arXiv:physics/0306116.
[30] L. Moneta *et al.*, arXiv:1009.1003 [physics].
[31] J. Heinrich and L. Lyons, Ann. Rev. Nucl. Part. Sci. **57**, 145 (2007).
[32] B. P. Roe, Nucl. Instrum. Meth. **A570**, 159 (2007).
[33] J. Beringer *et al.*, Phys. Rev. D **86**, 010001 (2012).
[34] S. A. Bass *et al.*, Prog. Part. Nucl. Phys. **41**, 255 (1998).
[35] H. Kamada, J. Golak, K. Miyagawa, H. Witala, and W. Glockle, Phys. Rev. C **57**, 1595 (1998).
[36] T. Motoba *et al.*, Nucl. Phys. A **534**, 597 (1991).
[37] I. Kumagai-Fuse and Y. Akaishi, Prog. Theor. Phys. **92**, 815 (1994).
[38] F. E. James, *Monte Carlo Phase Space CERN* (CERN, Geneva, Switzerland, 1968), p. 41.
[39] H. Outa *et al.*, Nucl. Phys. A **639**, 251C (1998).
[40] M. Juric *et al.*, Nucl. Phys. B **52**, 1 (1973).
[41] A. Gal (private communication).
[42] J. D. Parker *et al.*, Phys. Rev. C **76**, 035501 (2007).
[43] J. J. Szymanski *et al.*, Phys. Rev. C **43**, 849 (1991).
[44] S. Kameoka *et al.*, Nucl. Phys. A **754**, 173 (2005).
[45] A. Budzanowski *et al.*, Phys. Lett. B **687**, 31 (2010).
[46] A. Budzanowski *et al.*, Phys. Rev. D **84**, 032002 (2011).
[47] A. Gal, *From Nuclei to Stars*, edited by Sabine Lee (University of Birmingham, UK, 2011), pp. 157–170.